

# Learning Model Predictive Controllers with Real-Time Attention for Real-World Navigation

Xuesu Xiao<sup>\*1,2</sup>, Tingnan Zhang<sup>\*3</sup>, Krzysztof Choromanski<sup>\*3</sup>, Edward Lee<sup>3</sup>, Anthony Francis<sup>3</sup>, Jake Varley<sup>3</sup>, Stephen Tu<sup>3</sup>, Sumeet Singh<sup>3</sup>, Peng Xu<sup>3</sup>, Fei Xia<sup>3</sup>, Sven Mikael Persson<sup>2</sup>, Dmitry Kalashnikov<sup>3</sup>, Leila Takayama<sup>4</sup>, Roy Frostig<sup>3</sup>, Jie Tan<sup>3</sup>, Carolina Parada<sup>3</sup>, and Vikas Sindhwani<sup>3</sup>

<sup>\*</sup>Equally Contributing Authors <sup>1</sup>George Mason University

<sup>2</sup>Everyday Robots <sup>3</sup>Robotics@Google <sup>4</sup>Hoku Labs

**Abstract:** Despite decades of research, existing navigation systems still face real-world challenges when deployed in the wild, e.g., in cluttered home environments or in human-occupied public spaces. To address this, we present a new class of implicit control policies combining the benefits of imitation learning with the robust handling of system constraints from Model Predictive Control (MPC). Our approach, called Performer-MPC,<sup>1</sup> uses a learned cost function parameterized by vision context embeddings provided by Performers—a low-rank implicit-attention Transformer. We jointly train the cost function and construct the controller relying on it, effectively solving end-to-end the corresponding bi-level optimization problem. We show that the resulting policy improves standard MPC performance by leveraging a few expert demonstrations of the desired navigation behavior in different challenging real-world scenarios. Compared with a standard MPC policy, Performer-MPC achieves **>40%** better goal reached in cluttered environments and **>65%** better on social metrics when navigating around humans.

**Keywords:** Model Predictive Control, Transformers, Performers, Highly-Constrained Navigation, Social Navigation, Learning-based Control



Figure 1: Left: Standard MPC efficiently cuts blind corners, forcing the human to back up; Right: Social Performer-MPC avoids cutting blind corners, enabling safe navigation around humans.

## 1 Introduction and Related Work

Real-world robot deployment in human-centric environments, such as cluttered homes or crowded offices, remains an unsolved problem [1, 2]. These challenging situations require safe and efficient navigation through tight spaces, such as squeezing between coffee tables and couches, handling tight corners, doorways, untidy rooms, and so on. An equally critical requirement is to navigate in a manner that complies with unwritten social norms around humans.

Classical approaches using model-based control [3, 4, 5, 6] can already move robots from one point to another safely and reliably. However, when deploying these systems in the complex real world [7, 8, 9], extensive engineering effort is required to construct world representations [10, 11, 12], model vehicle kinodynamics [13, 14], hand-craft cost functions [15, 16], fine-tune system parameters [17],

<sup>1</sup>Project page: <https://performermpc.github.io>

and design backup planners to recover from stuck scenarios [18, 19, 20, 21]. While providing verifiable guarantees, these cascaded components need to be hand-engineered before deployment based on the roboticist’s best expectations of what would be encountered in the real world, and become cumbersome when in-situ modifications are necessary to enable adaptive behaviors [17].

In contrast to these classical methods, machine learning enables robots to *learn* these behaviors directly from data [22]. End-to-end learning [23, 24] is an appealing paradigm to reduce the engineering effort and cascading errors caused by separate components, but it usually requires extensive real-world training data or simulation with inevitably simplified human and environment representations. Most importantly, it lacks safety, optimality, generalizability, interpretability, and explainability, which are crucial for real robots moving around humans [22, 25, 26]. Therefore, researchers have looked at individually learning global planners [27], local planners [28, 29, 30, 31, 32, 33], and other navigation components including cost representations [34, 35, 36, 37], kinodynamic models [38, 39], and planner parameters [40, 41, 42, 43, 44, 45, 46] to enable both better navigation performance, and also off-road [47, 48] and social navigation [1, 49, 50].

Both classical and learning-based methods have their merits. Model Predictive Control (MPC) [3, 4, 5, 6] enables synthesis of real-time feedback controllers for robots operating in real-world environments that satisfy given safety constraints, optimality criteria, and kinodynamic models. To get the best of both worlds, we design a class of *Learnable-MPC* policies enabling robots to learn navigation behaviors in real-world use cases by combining the flexibility of learning from demonstrations with the optimality properties (e.g., collision-free, shortest path) of MPC solutions. Our framework can also be seen as a class of Implicit Behavior Cloning policies [51] that are aware of real-world robot-environment and robot-human interactions. Our contributions in this paper are three-fold:

- We augment the cost function of MPC with learnable components parameterized by rich Transformer-based latent embeddings of real-world context. Transformer architectures [52, 53, 54] have produced stunning advances in language modeling [55, 56, 57, 58, 59, 60], image generation [61, 62, 63, 64, 65, 66], and multi-modal reasoning [67, 68, 69, 70, 71, 72]. This indisputable success comes at a computational price in proportion to the massive number of parameters learned (e.g., 175 billion for GPT-3 [56]) as well as quadratic scaling in input sequence length of the core attention modules of these models. By generating context-dependent quadratic costs using Performers [73]—a low-rank linear-attention Transformer, we demonstrate how we can embed powerful *pixel-to-pixel* attention mechanisms in MPC while crucially retaining real-time solutions on a CPU onboard a mobile robot.
- Using distributed bilevel optimization with implicit differentiation mechanisms, we train navigation policies on expert demonstrations to handle difficult navigation scenarios, with data augmentation strategies to mitigate well-known distribution shift issues that frequently plague behavioral cloning and other imitation learning approaches.
- We demonstrate that our Performer-MPC outperforms its counterparts in real-world challenging navigation scenarios, including highly constrained and human-occupied environments. Performer-MPC learns to achieve >40% better goal reached in highly constrained environments and >65% better behavior as captured by social metrics defined in the Appendix when moving around humans in a social navigation pilot study.

## 2 Performer-MPC: Learnable MPC with Scalable Real-Time Attention

In order to respond to dynamic uncertainty in the environment, the principal challenges of synthesis of model predictive controllers [74, 75, 3] are: (i) to construct cost functions that remain suitable across a wide variety of robot-environment situations, and (ii) to generate reliable solutions to the underlying trajectory optimization problems in real-time. This work focuses on the first challenge above, in particular, by eschewing the classical approach of hand-engineered cost functions, and adopting a learning-based inverse optimal control [76, 77, 78, 79, 80, 81] framework, where the sensory/visual context is used to induce *what MPC problem to solve in real-time* in order to generate actions. We first provide some details on training and inference of a learnable MPC framework, and then discuss the details of the learnable components; see Fig. 2 for an overview.

### 2.1 Learnable Model Predictive Control

Let  $C_0$  denote the current “context”, e.g., such as a list of tensors encoding for example RGB/D streams, force-torque readings, and proprioceptive states over a short time-window. Consider a

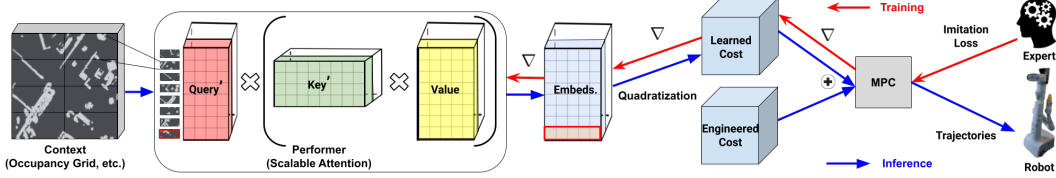


Figure 2: Overview of the Performer-MPC. The final latent embedding of the patch highlighted in red is used to construct context-dependent learnable cost. The backpropagation (red arrows) is through the parameters of the Transformer (see Sec. 2.2 for more details regarding Performers).

*Learnable-MPC* feedback policy implicitly defined by solving the following *parametric* optimal control problem at each time instant:

$$\arg \min_{\mathbf{u}_0 \dots \mathbf{u}_{T-1}} J_c(\mathbf{u}, \theta | C_0) = \sum_{t=0}^{T-1} c(\mathbf{x}_t, \mathbf{u}_t, t; C_0, \theta) + c_T(\mathbf{x}_T; C_0, \theta), \quad (1a)$$

$$\text{s.t.} \quad \mathbf{x}_{t+1} = f(\mathbf{x}_t, \mathbf{u}_t; \theta), \quad \mathbf{x}_0 = g(C_0, \theta) \text{ given.} \quad (1b)$$

Denote the optimizer as  $\mathbf{u}^*(\mathbf{x}_0; C_0, \theta)$ , and the corresponding optimal state sequence as  $\mathbf{x}^*(\mathbf{x}_0; C_0, \theta)$ . Here,  $\theta$  are learnable parameters for stagewise and terminal cost neural networks  $\{c, c_T\}$ ,  $f$  the dynamics function, and  $g$  current state estimator. While our framework generalizes to learning cost, dynamics, and state estimators simultaneously, in this paper we focus on the inverse optimal control setting: We study how the multi-layer self-attention cores of Transformers may be embedded in the *cost networks* to handle sensor fusion *while retaining real-time speed expectations of MPC*. The dynamics function here corresponds to the differential drive dynamics of our robot.

While the MPC-structured policy can be trained using any flavor of Reinforcement Learning, real-world trial-and-error data is prohibitively expensive and a general reward function that captures all intricacies of different real-world scenarios is difficult to design. Therefore, we take an Imitation Learning approach where the robot has access to  $N$  expert demonstrations. The MPC structure provides a form of a strong inductive bias for Imitation Learning, and can lead to improved data efficiency, robustness, and generalization. Denote  $\bar{\mathbf{u}}^i = (\bar{\mathbf{u}}_0^i, \dots, \bar{\mathbf{u}}_{T_i-1}^i)$  and  $\bar{\mathbf{x}}^i = (\bar{\mathbf{x}}_0^i, \dots, \bar{\mathbf{x}}_{T_i}^i)$  as the control and state sequence for the  $i^{\text{th}}$  demonstration snippet, with associated sensor context  $C_0^i$ , which can be extracted from offline planning or human teleoperation. We optimize  $\theta$  as follows:

$$\theta^* = \arg \min_{\theta} \sum_{i=1}^N J_l(\mathbf{u}^{i*}(\theta) | \bar{\mathbf{u}}^i, \bar{\mathbf{x}}^i), \quad (2)$$

where  $J_l$  denotes total imitation loss that measures discrepancy between MPC-generated and expert state-control trajectories. We assume that  $J_l$  also admits a stagewise and terminal decomposition using loss functions  $l$  and  $l_T$ :

$$J_l(\mathbf{u}^{i*}(\theta) | \bar{\mathbf{u}}^i, \bar{\mathbf{x}}^i) = \sum_{t=0}^{T_i-1} l(\mathbf{x}_t^{i*}(\theta), \mathbf{u}_t^{i*}(\theta), t, \bar{\mathbf{x}}_t^i, \bar{\mathbf{u}}_t^i) + l_T(\mathbf{x}_{T_i}^{i*}(\theta), \bar{\mathbf{x}}_{T_i}^i), \quad (3a)$$

$$\mathbf{x}_{t+1}^{i*}(\theta) = f(\mathbf{x}_t^{i*}(\theta), \mathbf{u}_t^{i*}(\theta)), \quad \mathbf{x}_0^{i*}(\theta) = \bar{\mathbf{x}}_0^i. \quad (3b)$$

Above,  $\mathbf{x}^{i*}$ ,  $\mathbf{u}^{i*}$  is the MPC solution with cost parameters  $\theta$ , given context  $C_0^i$  and initial state  $\bar{\mathbf{x}}_0^i$ .

**Training via Bilevel Optimization:** The training optimization problem in (3) has embedded the MPC optimization, (1). Together, the two may be viewed as an instance of *bilevel optimization*, where the higher-level searches for the best cost-network parameters  $\theta$  via imitation loss minimization, while the lower-level synthesizes the optimal predictive control sequences given fixed  $\theta$ . To use stochastic gradient descent for the higher-level problem, we need the gradient of  $J_l$  with respect to  $\theta$  evaluated at a control sequence  $\mathbf{u}^*(\theta_k)$  where  $\theta_k$  denotes the parameters during the current iterate  $k$  during training. This quantity decomposes as a vector-Jacobian product (VJP),

$$\nabla_{\theta} J_l(\mathbf{u}^*(\theta_k) | \bar{\mathbf{u}}^i, \bar{\mathbf{x}}^i) = \nabla_{\mathbf{u}} J_l(\mathbf{u}^*(\theta_k) | \bar{\mathbf{u}}^i, \bar{\mathbf{x}}^i)^T \partial_{\theta} \mathbf{u}^*(\theta_k). \quad (4)$$

The first term in the product on the right hand side is the gradient of the total imitation loss, which can be efficiently computed using the Adjoint method in Optimal Control [82] thanks to its stagewise

structure. The second term is the sensitivity of the MPC solution with respect to parameters, which may be efficiently computed using the Implicit Function Theorem (IFT), as featured in several works exploring differentiable “optimization layers” [83, 84, 85, 86], see Appendix for details.

**MPC Solver:** We use a second order Gauss-Newton trajectory optimizer [87, 88] called Iterative LQR (iLQR) [89] with line searches inspired by Differential Dynamic Programming (DDP) [90, 87]. At each iteration, iLQR quadratizes the cost and linearizes the dynamics to compute the search direction by solving a time-varying LQR (TVLQR) [82] problem. Upon convergence, a single additional LQR solve suffices for computing  $\partial_\theta \mathbf{u}^*(\theta)$  in (4).

**Policy:** While one may use the first component of the optimal solution for problem (1), i.e.,  $\mathbf{u}_0^*(\mathbf{x}_0; C_0, \theta)$ , as the policy map, we noted better performance by leveraging a secondary (non-learnable) MPC problem similar to (1), featuring a “tracking” objective w.r.t. the solution of the learnable MPC problem. The details of this “tracking MPC” problem are provided in the Appendix.

## 2.2 Attentive Cost Functions for Learnable MPC

We adopt an inverse optimal control framework for learnable MPC whereby only the cost function is learnable. We structure this cost as the sum of a user-engineered function and a context-dependent quadratic, parameterized by an embedding matrix  $\mathbf{P}$  and vector  $\mathbf{q}$  (described in more detail below):

$$c(\mathbf{x}, \mathbf{u}, t; C_0, \theta) = \bar{c}(\mathbf{x}, \mathbf{u}, t) + \begin{bmatrix} \mathbf{x} \\ \mathbf{u} \end{bmatrix}^T \mathbf{P}^T(C_0, \theta) \mathbf{P}(C_0, \theta) \begin{bmatrix} \mathbf{x} \\ \mathbf{u} \end{bmatrix} + \mathbf{q}(C_0, \theta)^T \begin{bmatrix} \mathbf{x} \\ \mathbf{u} \end{bmatrix}. \quad (5)$$

Here,  $\bar{c}$  refers to the hand-designed cost function (see Appendix), appended to a Transformer-backed cost model that attends to the current context  $C_0$  to generate residual quadratic cost terms for MPC to optimize. This structure removes the computational cost of repeated quadratization of a large network in the iLQR solver. Furthermore, since the residual cost is convex and well-conditioned, crude MPC solutions can generate reliable descent directions for the higher-level optimizer, even though applying IFT in gradient computation assumes the MPC solution is precisely a local minimum. We next describe the details of the embeddings  $\mathbf{P}$  and  $\mathbf{q}$ .

**Generating Context-Dependent Transformer Embeddings:** We outline a general Transformer-based backend for learnable-MPCs which leads to Performer-MPCs. The backend maps the current contexts  $C_0$  into a latent embedding which can be reshaped into the matrices  $\mathbf{P}$  and  $\mathbf{q}$  to support the quadratic parameterization of Eqn. 5. For concreteness, let  $C_0$  be an image frame, i.e., the occupancy grid in the robot frame. As in Vision Transformer architectures [91, 92, 93], each frame is first independently pre-processed by a convolution layer, and then flattened to a sequence. Each element (token) of the sequence corresponds to a different patch of the original frame which is then enriched with positional encodings. The length  $L$  of this sequence is a patch-size hyper-parameter. The preprocessed input is then fed to regular attention and MLP layers. The final embedding of one of the tokens is chosen as a latent representation of the entire context  $C_0$  to parameterize the learnable cost (e.g., via de-vectorization to  $\mathbf{P}$  and  $\mathbf{q}$  as in Eqn. 5). Even though we take the final embedding of a single token, it contains signal from all the tokens since attention mixes information across tokens.

The attention used in regular Transformer architectures [52] linearly projects tokens’ embeddings (via trainable transformations) into three matrices,  $\mathbf{Q}, \mathbf{K}, \mathbf{V} \in \mathbb{R}^{L \times d}$ , called *queries*, *keys* and *values* respectively. The output of the attention is then defined as:

$$\text{Att}(\mathbf{Q}, \mathbf{K}, \mathbf{V}) = \mathbf{D}^{-1} \mathbf{A} \mathbf{V}, \quad \mathbf{A} = \exp(\mathbf{Q} \mathbf{K}^T / \sqrt{d}), \quad \mathbf{D} = \text{diag}(\mathbf{A} \mathbf{1}_L), \quad (6)$$

where  $\mathbf{A} \in \mathbb{R}^{L \times L}$  is called the *attention matrix*. In the above formula,  $\exp(\cdot)$  is applied element-wise,  $\mathbf{1}_L$  is the all-ones vector of length  $L$ , and  $\text{diag}(\cdot)$  is a diagonal matrix with the input vector as the diagonal. Space and time complexity of computing Eqn. 6 are:  $O(L^2 + Ld)$  and  $O(L^2d)$  respectively, because  $\mathbf{A}$  has to be explicitly stored. Quadratic time and space complexity in the number of patches makes this approach prohibitive for real-time robotic navigation. To address this, we apply a class of low-rank implicit linear-attention Transformer architectures, called *Performers* [73].

Performers interpret attention matrices  $\mathbf{A} \in \mathbb{R}^{L \times L}$  as kernel matrices, i.e.,  $\mathbf{A}(i, j)$  is defined as:  $\mathbf{A}(i, j) = \mathbf{K}(\mathbf{q}_i, \mathbf{k}_j)$ , with  $\mathbf{q}_i/\mathbf{k}_j$  standing for the  $i^{\text{th}}/j^{\text{th}}$  query/key row-vector in  $\mathbf{Q}/\mathbf{K}$  and kernel

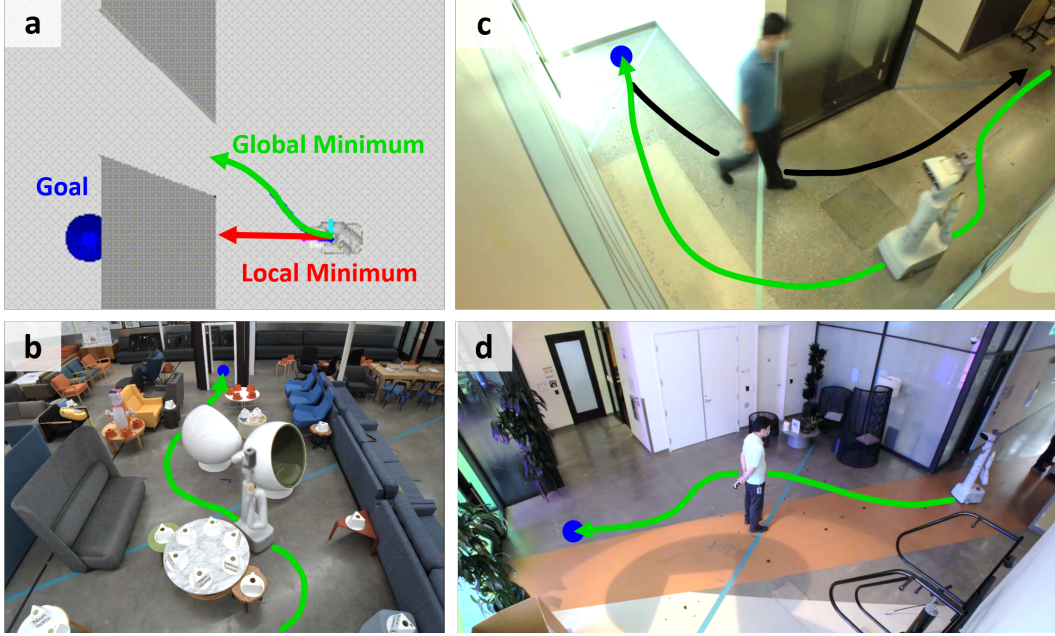


Figure 3: Experiment Scenarios: (a) Learning to avoid local minima during doorway traversal, (b) to maneuver through highly constrained spaces, and (c) to enable socially compliant behaviors for blind corner and (d) pedestrian obstruction interactions.

$\mathbf{K} : \mathbb{R}^d \times \mathbb{R}^d \rightarrow \mathbb{R}_+$  defined for the (randomized) mapping  $\phi : \mathbb{R}^d \rightarrow \mathbb{R}^m$  (for  $m > 0$ ) as:

$$\mathbf{K}(\mathbf{x}, \mathbf{y}) = \mathbb{E}[\phi(\mathbf{x})^\top \phi(\mathbf{y})]. \quad (7)$$

We call  $\phi(\mathbf{v})$  a (random) feature map for  $\mathbf{v} \in \mathbb{R}^d$ . For  $\mathbf{Q}', \mathbf{K}' \in \mathbb{R}^{L \times m}$  with rows given as  $\phi(\mathbf{q}_i)$  and  $\phi(\mathbf{k}_i)$  respectively, Eqn. 7 leads directly to the efficient attention mechanism of the form:

$$\widehat{\text{Att}}(\mathbf{Q}, \mathbf{K}, \mathbf{V}) = \widehat{\mathbf{D}}^{-1}(\mathbf{Q}'((\mathbf{K}')^\top \mathbf{V})), \quad \widehat{\mathbf{D}} = \text{diag}(\mathbf{Q}'((\mathbf{K}')^\top \mathbf{1}_L)). \quad (8)$$

Here  $\widehat{\text{Att}}$  stands for the approximate attention and the parentheses indicate the order of computations. Such a mechanism is characterized by space complexity of  $O(Lm + Ld + md)$  and time complexity of  $O(Lmd)$  as opposed to  $O(L^2 + Ld)$  and  $O(L^2d)$  of the regular attention mechanism. Different mappings  $\phi$  give rise to different Performer variants. Two most popular ones [73] are:

$$\begin{aligned} \phi_{\text{exp}}(\mathbf{x}) &\stackrel{\text{def}}{=} \frac{1}{\sqrt{m}} \exp\left(-\frac{\|\mathbf{x}\|_2^2}{2}\right) (\exp(\omega_1^\top \mathbf{x}), \dots, \exp(\omega_m^\top \mathbf{x})) \text{ and,} \\ \phi_{\text{relu}}(\mathbf{x}) &\stackrel{\text{def}}{=} \frac{1}{\sqrt{m}} (\text{ReLU}(x_1), \dots, \text{ReLU}(x_d)) \text{ (with } m = d), \end{aligned} \quad (9)$$

for  $\omega_1, \dots, \omega_m \sim \mathcal{N}(0, \mathbf{I}_d)$  and we will refer to the corresponding Performers as *Performer-Exp* and *Performer-ReLU* respectively. Mapping  $\phi_{\text{exp}}$  provides unbiased estimation of the softmax attention-kernel from Eqn. 5, but requires random projections, whereas  $\phi_{\text{relu}}$  defines weaker attention-kernel, but does not use random projections and leads to the fastest Performer variant. In Section 3.2 and the Appendix, we provide a comprehensive speed benchmark for Performer-MPC variations, demonstrating Pixel-to-Pixel attention at real-time speeds.

### 3 Experiments

Our Performer-MPC is tested on a differential-drive wheeled robot, which has a 3D LiDAR in the front, and depth sensors mounted on its head (see Fig. 1). It is a three-layer Performer-ReLU model with  $\text{mlpdim} = 64$  and one head. Our policies are trained on four TPUs and then deployed on a CPU onboard the robot. We use the differentiable Iterative LQR implementation of trajax [94] for MPC training and inference. Please refer to the Appendix for more details.

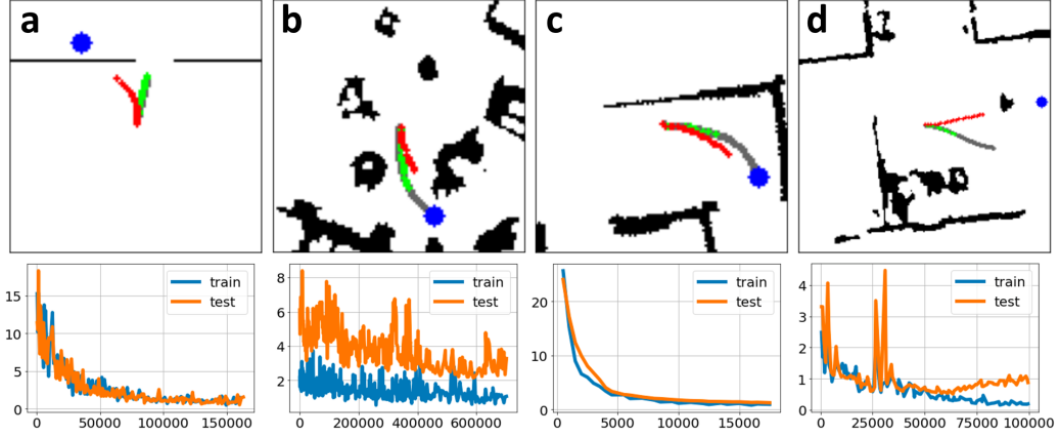


Figure 4: Top: Visualization of test data examples in the (a) doorway traversal, (b) highly constrained obstacle course, (c) blind corner, and (d) pedestrian obstruction scenarios. Performer-MPC trajectories aiming at the goal are always closer to the expert demonstrations compared to the RMPC trajectories. Bottom: Train and test curves, where the vertical axis represents loss values (Hausdorff distance to the expert trajectories) and horizontal axis represents training steps.

Performer-MPC is compared with two baselines, a regular MPC policy (RMPC) without the learned cost components, and an Explicit Policy (EP) that predicts a reference/goal state using the same Performer architecture, but without being coupled to the MPC structure. The control action (i.e., final policy output) is implicitly defined via the solution of the “tracking MPC” problem (see previous section), where the reference trajectory is generated by one of RMPC, EP, or Performer-MPC.

We evaluate our method in four scenarios, one in simulation and three in the real world (Fig. 3). For each scenario, the learned policies (EP and Performer-MPC) are trained with demonstrations specifically collected for that scenario. To address the distribution shift issue, we not only collect positive examples where the robot is driving smoothly with the intended behavior, but also start the robot in randomly selected “disadvantage locations” (e.g., near-collision situations), and steer the robot to recover from them. For more data collection details please refer to the Appendix. We visualize the planning results of Performer-MPC (green) and RMPC (red) along with expert demonstrations (grey) in the top half of Fig. 4 and the train and test curves in the bottom half.

### 3.1 Experimental Results

**Learning to Avoid Local Minima:** We first evaluate our method in a simulated doorway traversal scenario (Fig. 3a). 100 start and goal pairs are randomly sampled from opposing sides of the wall. A planner guided by a greedy cost function often leads the robot to a local minimum, i.e., getting stuck at the closest point to the goal on the other side of the wall. Although such a problem can be mitigated by using a global planner, we use this as a test case to showcase the learning results. We generate 2000 expert demonstrations using an off-line iLQR planner [89], which iteratively solves for intermediate way points provided by a Dijkstra’s global planner. Using these off-line demonstrations, Performer-MPC learns a cost landscape that steers the robot towards the doorway, even if it must veer away from the goal and travel further. Performer-MPC passes the doorway in 86 out of 100 trials while RMPC only passes 24 out of 100.

**Learning Highly-Constrained Maneuvers:** We next test our method in a challenging real-world scenario—a cluttered home/office setting where the robot must perform sharp, near-collision maneuvers (Fig. 3b). A global planner provides coarse way points for the robot to follow. Each policy is run ten times and we report Success Rate (SR) and average Completion Percentage (CP) with variance (VAR) of the obstacle course that the robot is able to traverse without collisions or getting stuck (Fig. 5). Performer-MPC outperforms both RMPC and EP in SR and CP.

**Learning to Anticipate Pedestrians at Blind Corners:** Going beyond static obstacles, we apply our method to social robot navigation [1], where robots must respect unwritten social norms for which cost functions are hard to design. One such scenario is blind corner (Fig. 3c), where robots

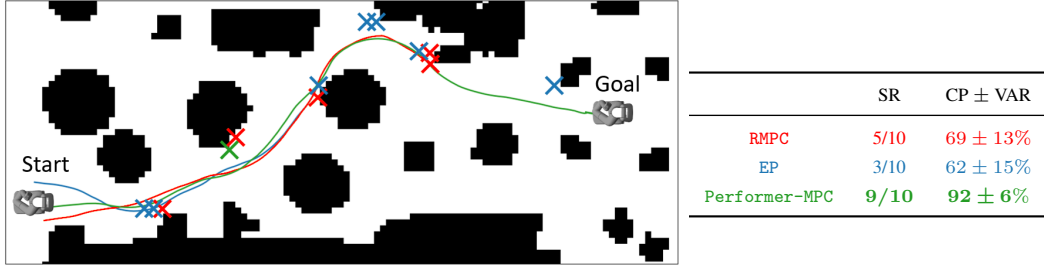


Figure 5: A  $4.5 \times 10$  m<sup>2</sup> obstacle course with policy trajectories and failure locations indicated by crosses for RMPC, EP, and Performer-MPC.

should avoid the inner side of a hallway corner in case a human suddenly appears in this “blind spot”. For blind corner, we collect 30 demonstrations with a human driving the robot from a randomly chosen location on one side of the corner to the other side in a socially compliant manner. After training, we evaluate each policy twenty times in the real world: ten times in the corner where the demonstrations were collected (seen), and ten times in a different corner (unseen). During each run, the robot and a pedestrian human subject will approach the corner from opposite sides, while a third-party observer monitors from a distance. We use a social navigation evaluation protocol [95] in which pedestrians and observers rate the performance of the policy using a standardized questionnaire scored with Likert scales [96] which we combine into a joint social navigation score (see Appendix for further details). Social navigation scores for blind corner seen and unseen scenarios are shown in Fig. 6a. RMPC has the least social compliance: its hand-crafted cost function efficiently cuts the corner, causing uncomfortable near-collisions (Fig. 1). EP performs slightly better than Performer-MPC in the seen environments, but does not generalize well to unseen scenarios, with worse social scores and a 20% failure rate (e.g., safety stops or not reaching the goal).

**Learning to Respect Comfort Distance When Obstructed by Pedestrians:** Another common social navigation scenario is pedestrian obstruction, when a human unexpectedly impedes the prescribed path of a robot (Fig. 3d). While static obstacle avoidance is a largely solved problem, pedestrian obstruction is particularly challenging for MPC policies that are guided by waypoints that were valid before the human entered the environment. A hand-crafted cost function may guide the robot too near to the human, causing uncomfortably close interactions or the robot getting stuck right in front of the human. We evaluate policy performance for pedestrian obstruction using the social navigation evaluation protocol [95]. Again, Performer-MPC is the most socially compliant (Fig. 6b), and in a few cases even shows emergent maneuvers unseen in the dataset (i.e., passing the human on the left if there is not enough space on the right, while the demonstrations only include right-side passing). In contrast, RMPC usually gets stuck in front of the human due to a local minimum close to the goal behind the human. While EP does stay away from the human

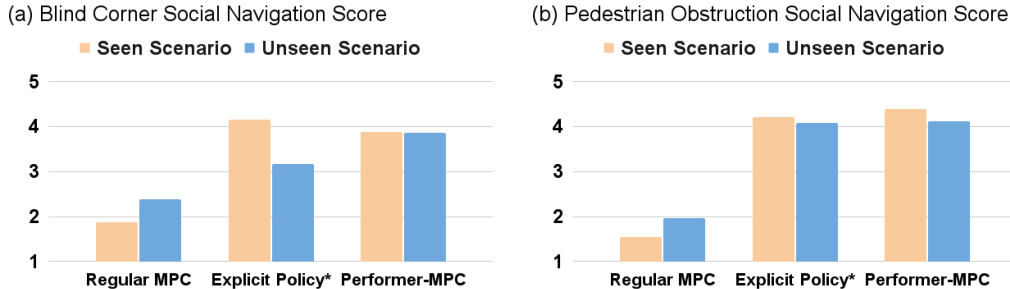


Figure 6: Social Navigation Results. (a) In the blind corner scenario, Performer-MPC achieves a better social navigation score than RMPC and similar to EP in the seen environment. In the unseen environment Performer-MPC is better than both baselines. EP fails to complete unseen 20% of the time (e.g., not reaching the goal or triggering a safety stop, denoted by \*). (b) In the pedestrian obstruction scenario, both EP and Performer-MPC show similar social scores and are superior to RMPC, but EP fails in seen or unseen conditions 5% of the time (again denoted by \*). Performer-MPC thus shows better generalizability in both social score and navigation success.

subject in both *seen* and *unseen*, it struggles to reach the goal location and sometimes comes close to colliding with nearby walls, leading to a 5% overall failure rate. Please refer to the Appendix for a detailed description of both social scenarios and statistical analysis of the results.

### 3.2 Speed Studies Over Various Performer Architectures

Below we present speed ablation studies over various Performer architectures leading to Performer-ReLU as a default choice. More detailed studies are given in the Appendix. Tests presented here are run on  $100 \times 100$  images, with patch size  $5 \times 5$  and two architecture sizes: (a) **medium** with  $l = 3$  layers,  $h = 1$  head, and  $\text{mlpdim} = 64$  (8.3M parameters) and (b) **large** with  $l = 6$  layers,  $h = 3$  heads, and  $\text{mlpdim} = 1024$  (24.6M parameters). We benchmark Performer-ReLU and Performer-Exp (for the latter one varying the number of random projections *rps* used and either redrawing them or not at each forward pass), measuring wall-clock time taken by the MPC. For the fastest Performer-ReLU variant, we run additional studies (this time measuring CPU-time to distill time taken solely by the MPC from I/O time, etc.) for varying patch sizes, showing that *we can reach Pixel-to-Pixel attention with near real-time speed* (11.3ms per MPC iteration). The results are presented in tables Tab. 1 and 2.

Table 1: Speed ablation tests for different variants of Performers with  $100 \times 100$  input images. The architecture deployed on the real robot is denoted in **bold**.

model size	Performer type	redraw	rps #	wall-clock time per MPC-iteration [ms]
<b>medium</b>	<b>ReLU</b>	<b>N/A</b>	<b>N/A</b>	<b>8.3</b>
medium	Exp	False	8	21.5
medium	Exp	False	16	21.6
medium	Exp	False	64	23.6
large	ReLU	N/A	N/A	13.8
large	Exp	False	8	72.9
large	Exp	False	16	66.9
large	Exp	False	64	83.0

Table 2: Speed ablation over patch sizes for medium-sized Performer-ReLU with  $100 \times 100$  inputs.

patch sizes	$1 \times 1$	$2 \times 2$	$4 \times 4$	$5 \times 5$	$10 \times 10$
number of params (M)	15.7	9.93	8.50	8.33	8.16
CPU-time per MPC-iteration (ms)	11.3	2.6	2.3	1.5	0.5

## 4 Limitations

Currently our Transformer-backend uses spatial attention, but in principle it can leverage the temporal axis. For example, in a face-to-face approach with a walking human in a hallway, motion history may shed light on how the human intends to move in the future, e.g., yielding left or right. A promising future research direction is to add history dependency so that the robot can sequentially reason about potential future interactions and conflicts. Furthermore, exploring richer modalities [97] than the occupancy grid (e.g., RGB images, human traces, language contexts [98, 72]), to enable robot-environment and robot-human interactions beyond simple geometry is another natural way to extend our approach. Another limitation is while the quadratic cost assures global convexity and training stability, it limits the expressiveness and complexity of the cost function. Furthermore, the cost function is learned individually for each navigation scenario, but it is unclear how one stand-alone learned cost function can handle multiple scenarios. Also, our user study pilot questionnaire could be refined, and our social evaluations could be expanded to a broader set of scenarios.

## 5 Conclusions

We present in this paper Performer-MPC, a learnable MPC system utilizing scalable Transformers to learn rich context representations parameterizing trainable cost function. We show that Performer-MPCs can be used as robotic controllers for navigation in challenging real-world environments where regular MPCs struggle, including learning to avoid local minima, to maneuver through highly constrained spaces, and to adhere to unwritten social norms, while maintaining real-time speed, even for nearly Pixel-to-Pixel attention.



## References

- [1] C. Mavrogiannis, F. Baldini, A. Wang, D. Zhao, P. Trautman, A. Steinfeld, and J. Oh. Core challenges of social robot navigation: A survey. *arXiv preprint arXiv:2103.05668*, 2021.
- [2] X. Xiao, Z. Xu, Z. Wang, Y. Song, G. Warnell, P. Stone, T. Zhang, S. Ravi, G. Wang, H. Karnan, et al. Autonomous ground navigation in highly constrained spaces: Lessons learned from the barn challenge at icra 2022. *arXiv preprint arXiv:2208.10473*, 2022.
- [3] C. E. Garcia, D. M. Prett, and M. Morari. Model predictive control: Theory and practice—a survey. *Automatica*, 25(3):335–348, 1989.
- [4] Y. Wang and S. Boyd. Fast model predictive control using online optimization. *IEEE Transactions on control systems technology*, 18(2):267–278, 2009.
- [5] S. Maniatopoulos, D. Panagou, and K. J. Kyriakopoulos. Model predictive control for the navigation of a nonholonomic vehicle with field-of-view constraints. In *2013 American control conference*, pages 3967–3972. IEEE, 2013.
- [6] T. Fork, H. E. Tseng, and F. Borrelli. Models and predictive control for nonplanar vehicle navigation. In *2021 IEEE International Intelligent Transportation Systems Conference (ITSC)*, pages 749–754. IEEE, 2021.
- [7] Everyday Robots. Everyday robots. <https://everydayrobots.com/>, 2022.
- [8] Amazon. Meet scout. <https://www.aboutamazon.com/news/transportation/meet-scout>, 2022.
- [9] Starship. Starship. <https://www.starship.xyz/>, 2022.
- [10] A. Elfes. A tessellated probabilistic representation for spatial robot perception and navigation. In *JPL, California Inst. of Tech., Proceedings of the NASA Conference on Space Telerobotics, Volume 2*, 1989.
- [11] A. Elfes. Using occupancy grids for mobile robot perception and navigation. *Computer*, 22(6):46–57, 1989.
- [12] F. Dellaert, M. Kaess, et al. Factor graphs for robot perception. *Foundations and Trends® in Robotics*, 6(1-2):1–139, 2017.
- [13] S. Rabiee and J. Biswas. A friction-based kinematic model for skid-steer wheeled mobile robots. In *2019 International Conference on Robotics and Automation (ICRA)*, pages 8563–8569. IEEE, 2019.
- [14] Y. Tian and N. Sarkar. Control of a mobile robot subject to wheel slip. *Journal of Intelligent & Robotic Systems*, 74(3):915–929, 2014.
- [15] D. V. Lu, D. Hershberger, and W. D. Smart. Layered costmaps for context-sensitive navigation. In *2014 IEEE/RSJ International Conference on Intelligent Robots and Systems*, pages 709–715. IEEE, 2014.
- [16] L. Jaillet, J. Cortés, and T. Siméon. Sampling-based path planning on configuration-space costmaps. *IEEE Transactions on Robotics*, 26(4):635–646, 2010.
- [17] K. Zheng. Ros navigation tuning guide. In *Robot Operating System (ROS)*, pages 197–226. Springer, 2021.
- [18] OSRF. Ros wiki move\_base. [http://wiki.ros.org/move\\_base](http://wiki.ros.org/move_base), 2018. Accessed: 2022-06-12.
- [19] M. McNaughton, C. Urmson, J. M. Dolan, and J.-W. Lee. Motion planning for autonomous driving with a conformal spatiotemporal lattice. In *2011 IEEE International Conference on Robotics and Automation*, pages 4889–4895. IEEE, 2011.
- [20] D. Fox, W. Burgard, and S. Thrun. The dynamic window approach to collision avoidance. *IEEE Robotics & Automation Magazine*, 4(1):23–33, 1997.

- [21] S. Quinlan and O. Khatib. Elastic bands: Connecting path planning and control. In *[1993] Proceedings IEEE International Conference on Robotics and Automation*, pages 802–807. IEEE, 1993.
- [22] X. Xiao, B. Liu, G. Warnell, and P. Stone. Motion planning and control for mobile robot navigation using machine learning: a survey. *Autonomous Robots*, pages 1–29, 2022.
- [23] M. Bojarski, D. Del Testa, D. Dworakowski, B. Firner, B. Flepp, P. Goyal, L. D. Jackel, M. Monfort, U. Muller, J. Zhang, et al. End to end learning for self-driving cars. *arXiv preprint arXiv:1604.07316*, 2016.
- [24] M. Pfeiffer, M. Schaeuble, J. Nieto, R. Siegwart, and C. Cadena. From perception to decision: A data-driven approach to end-to-end motion planning for autonomous ground robots. In *2017 IEEE International Conference on Robotics and Automation (ICRA)*, pages 1527–1533. IEEE, 2017.
- [25] Z. Xu, X. Xiao, G. Warnell, A. Nair, and P. Stone. Machine learning methods for local motion planning: A study of end-to-end vs. parameter learning. In *2021 IEEE International Symposium on Safety, Security, and Rescue Robotics (SSRR)*, pages 217–222. IEEE, 2021.
- [26] Z. Xu, B. Liu, X. Xiao, A. Nair, and P. Stone. Benchmarking reinforcement learning techniques for autonomous navigation. Technical report, The University of Texas at Austin, 2022.
- [27] X. Yao, J. Zhang, and J. Oh. Following social groups: Socially compliant autonomous navigation in dense crowds. *arXiv preprint arXiv:1911.12063*, 2019.
- [28] A. Faust, K. Oslund, O. Ramirez, A. Francis, L. Tapia, M. Fiser, and J. Davidson. Prm-rl: Long-range robotic navigation tasks by combining reinforcement learning and sampling-based planning. In *2018 IEEE International Conference on Robotics and Automation (ICRA)*, pages 5113–5120. IEEE, 2018.
- [29] H.-T. L. Chiang, A. Faust, M. Fiser, and A. Francis. Learning navigation behaviors end-to-end with autorl. *IEEE Robotics and Automation Letters*, 4(2):2007–2014, 2019.
- [30] X. Xiao, B. Liu, G. Warnell, and P. Stone. Toward agile maneuvers in highly constrained spaces: Learning from hallucination. *IEEE Robotics and Automation Letters*, 6(2):1503–1510, 2021.
- [31] X. Xiao, B. Liu, and P. Stone. Agile robot navigation through hallucinated learning and sober deployment. In *2021 IEEE International Conference on Robotics and Automation (ICRA)*, pages 7316–7322. IEEE, 2021.
- [32] Z. Wang, X. Xiao, A. J. Nettekoven, K. Umasankar, A. Singh, S. Bommakanti, U. Topcu, and P. Stone. From agile ground to aerial navigation: Learning from learned hallucination. In *2021 IEEE/RSJ International Conference on Intelligent Robots and Systems (IROS)*, pages 148–153. IEEE, 2021.
- [33] B. Liu, X. Xiao, and P. Stone. A lifelong learning approach to mobile robot navigation. *IEEE Robotics and Automation Letters*, 6(2):1090–1096, 2021.
- [34] K. S. Sikand, S. Rabiee, A. Uccello, X. Xiao, G. Warnell, and J. Biswas. Visual representation learning for preference-aware path planning. In *2022 IEEE International Conference on Robotics and Automation (ICRA)*. IEEE, 2022.
- [35] P. Drews, G. Williams, B. Goldfain, E. A. Theodorou, and J. M. Rehg. Aggressive deep driving: Model predictive control with a cnn cost model. *arXiv preprint arXiv:1707.05303*, 2017.
- [36] M. Wigness, J. G. Rogers, and L. E. Navarro-Serment. Robot navigation from human demonstration: Learning control behaviors. In *2018 IEEE International Conference on Robotics and Automation (ICRA)*, pages 1150–1157. IEEE, 2018.
- [37] B. Kim and J. Pineau. Socially adaptive path planning in human environments using inverse reinforcement learning. *International Journal of Social Robotics*, 8(1):51–66, 2016.

- [38] H. Karnan, K. S. Sikand, P. Atreya, S. Rabiee, X. Xiao, G. Warnell, P. Stone, and J. Biswas. Vi-ikd: High-speed accurate off-road navigation using learned visual-inertial inverse kinodynamics. *arXiv preprint arXiv:2203.15983*, 2022.
- [39] X. Xiao, J. Biswas, and P. Stone. Learning inverse kinodynamics for accurate high-speed off-road navigation on unstructured terrain. *IEEE Robotics and Automation Letters*, 6(3):6054–6060, 2021.
- [40] D. Teso-Fz-Betoño, E. Zulueta, U. Fernandez-Gamiz, A. Saenz-Aguirre, and R. Martinez. Predictive dynamic window approach development with artificial neural fuzzy inference improvement. *Electronics*, 8(9):935, 2019.
- [41] M. Bhardwaj, B. Boots, and M. Mukadam. Differentiable gaussian process motion planning. In *2020 IEEE International Conference on Robotics and Automation (ICRA)*, pages 10598–10604. IEEE, 2020.
- [42] X. Xiao, Z. Wang, Z. Xu, B. Liu, G. Warnell, G. Dhamankar, A. Nair, and P. Stone. Appl: Adaptive planner parameter learning. *Robotics and Autonomous Systems*, 154:104132, 2022.
- [43] X. Xiao, B. Liu, G. Warnell, J. Fink, and P. Stone. Appld: Adaptive planner parameter learning from demonstration. *IEEE Robotics and Automation Letters*, 5(3):4541–4547, 2020.
- [44] Z. Wang, X. Xiao, B. Liu, G. Warnell, and P. Stone. Appli: Adaptive planner parameter learning from interventions. In *2021 IEEE International Conference on Robotics and Automation (ICRA)*, pages 6079–6085. IEEE, 2021.
- [45] Z. Wang, X. Xiao, G. Warnell, and P. Stone. Apple: Adaptive planner parameter learning from evaluative feedback. *IEEE Robotics and Automation Letters*, 6(4):7744–7749, 2021.
- [46] Z. Xu, G. Dhamankar, A. Nair, X. Xiao, G. Warnell, B. Liu, Z. Wang, and P. Stone. Applr: Adaptive planner parameter learning from reinforcement. In *2021 IEEE International Conference on Robotics and Automation (ICRA)*, pages 6086–6092. IEEE, 2021.
- [47] M. Bajracharya, A. Howard, L. H. Matthies, B. Tang, and M. Turmon. Autonomous off-road navigation with end-to-end learning for the lagr program. *Journal of Field Robotics*, 26(1): 3–25, 2009.
- [48] J. A. Bagnell, D. Bradley, D. Silver, B. Sofman, and A. Stentz. Learning for autonomous navigation. *IEEE Robotics & Automation Magazine*, 17(2):74–84, 2010.
- [49] R. Mirsky, X. Xiao, J. Hart, and P. Stone. Prevention and resolution of conflicts in social navigation—a survey. *arXiv preprint arXiv:2106.12113*, 2021.
- [50] V. Tolani, S. Bansal, A. Faust, and C. Tomlin. Visual navigation among humans with optimal control as a supervisor. *IEEE Robotics and Automation Letters*, 6(2):2288–2295, 2021.
- [51] P. Florence, C. Lynch, A. Zeng, O. A. Ramirez, A. Wahid, L. Downs, A. Wong, J. Lee, I. Mordatch, and J. Tompson. Implicit behavioral cloning. In *Conference on Robot Learning*, pages 158–168. PMLR, 2022.
- [52] A. Vaswani, N. Shazeer, N. Parmar, J. Uszkoreit, L. Jones, A. N. Gomez, Ł. Kaiser, and I. Polosukhin. Attention is all you need. *Advances in neural information processing systems*, 30, 2017.
- [53] J. Devlin, M.-W. Chang, K. Lee, and K. Toutanova. Bert: Pre-training of deep bidirectional transformers for language understanding. *arXiv preprint arXiv:1810.04805*, 2018.
- [54] T. Lin, Y. Wang, X. Liu, and X. Qiu. A survey of transformers. *arXiv preprint arXiv:2106.04554*, 2021.
- [55] A. Chowdhery, S. Narang, J. Devlin, M. Bosma, G. Mishra, A. Roberts, P. Barham, H. W. Chung, C. Sutton, S. Gehrmann, et al. Palm: Scaling language modeling with pathways. *arXiv preprint arXiv:2204.02311*, 2022.

- [56] T. Brown, B. Mann, N. Ryder, M. Subbiah, J. D. Kaplan, P. Dhariwal, A. Neelakantan, P. Shyam, G. Sastry, A. Askell, et al. Language models are few-shot learners. *Advances in neural information processing systems*, 33:1877–1901, 2020.
- [57] N. Du, Y. Huang, A. M. Dai, S. Tong, D. Lepikhin, Y. Xu, M. Krikun, Y. Zhou, A. W. Yu, O. Firat, et al. Glam: Efficient scaling of language models with mixture-of-experts. In *International Conference on Machine Learning*, pages 5547–5569. PMLR, 2022.
- [58] J. W. Rae, S. Borgeaud, T. Cai, K. Millican, J. Hoffmann, F. Song, J. Aslanides, S. Henderson, R. Ring, S. Young, et al. Scaling language models: Methods, analysis & insights from training gopher. *arXiv preprint arXiv:2112.11446*, 2021.
- [59] S. Smith, M. Patwary, B. Norick, P. LeGresley, S. Rajbhandari, J. Casper, Z. Liu, S. Prabh-moye, G. Zerveas, V. Korthikanti, et al. Using deepspeed and megatron to train megatron-turing nlg 530b, a large-scale generative language model. *arXiv preprint arXiv:2201.11990*, 2022.
- [60] R. Thoppilan, D. De Freitas, J. Hall, N. Shazeer, A. Kulshreshtha, H.-T. Cheng, A. Jin, T. Bos, L. Baker, Y. Du, et al. Lamda: Language models for dialog applications. *arXiv preprint arXiv:2201.08239*, 2022.
- [61] B. Zhang, S. Gu, B. Zhang, J. Bao, D. Chen, F. Wen, Y. Wang, and B. Guo. Styleswin: Transformer-based gan for high-resolution image generation. In *Proceedings of the IEEE/CVF Conference on Computer Vision and Pattern Recognition*, pages 11304–11314, 2022.
- [62] P. Esser, R. Rombach, and B. Ommer. Taming transformers for high-resolution image synthesis. In *Proceedings of the IEEE/CVF conference on computer vision and pattern recognition*, pages 12873–12883, 2021.
- [63] M. Chen, A. Radford, R. Child, J. Wu, H. Jun, D. Luan, and I. Sutskever. Generative pretraining from pixels. In *International conference on machine learning*, pages 1691–1703. PMLR, 2020.
- [64] L. Zhao, Z. Zhang, T. Chen, D. Metaxas, and H. Zhang. Improved transformer for high-resolution gans. *Advances in Neural Information Processing Systems*, 34:18367–18380, 2021.
- [65] K. Lee, H. Chang, L. Jiang, H. Zhang, Z. Tu, and C. Liu. Vitgan: Training gans with vision transformers. *arXiv preprint arXiv:2107.04589*, 2021.
- [66] Y. Jiang, S. Chang, and Z. Wang. Transgan: Two pure transformers can make one strong gan, and that can scale up. *Advances in Neural Information Processing Systems*, 34:14745–14758, 2021.
- [67] J.-B. Alayrac, J. Donahue, P. Luc, A. Miech, I. Barr, Y. Hasson, K. Lenc, A. Mensch, K. Millican, M. Reynolds, et al. Flamingo: a visual language model for few-shot learning. *arXiv preprint arXiv:2204.14198*, 2022.
- [68] A. Radford, J. W. Kim, C. Hallacy, A. Ramesh, G. Goh, S. Agarwal, G. Sastry, A. Askell, P. Mishkin, J. Clark, et al. Learning transferable visual models from natural language supervision. In *International Conference on Machine Learning*, pages 8748–8763. PMLR, 2021.
- [69] J. Wang, Z. Yang, X. Hu, L. Li, K. Lin, Z. Gan, Z. Liu, C. Liu, and L. Wang. Git: A generative image-to-text transformer for vision and language. *arXiv preprint arXiv:2205.14100*, 2022.
- [70] R. Hu and A. Singh. Unit: Multimodal multitask learning with a unified transformer. In *Proceedings of the IEEE/CVF International Conference on Computer Vision*, pages 1439–1449, 2021.
- [71] V. Likhoshesterov, A. Arnab, K. Choromanski, M. Lucic, Y. Tay, A. Weller, and M. Dehghani. Polyvit: Co-training vision transformers on images, videos and audio. *arXiv preprint arXiv:2111.12993*, 2021.
- [72] A. Zeng, A. Wong, S. Welker, K. Choromanski, F. Tombari, A. Purohit, M. Ryoo, V. Sindhwani, J. Lee, V. Vanhoucke, et al. Socratic models: Composing zero-shot multimodal reasoning with language. *arXiv preprint arXiv:2204.00598*, 2022.

- [73] K. M. Choromanski, V. Likhoshesterov, D. Dohan, X. Song, A. Gane, T. Sarlós, P. Hawkins, J. Q. Davis, A. Mohiuddin, L. Kaiser, D. B. Belanger, L. J. Colwell, and A. Weller. Rethinking attention with performers. In *9th International Conference on Learning Representations, ICLR 2021, Virtual Event, Austria, May 3-7, 2021*, 2021.
- [74] F. Borrelli, A. Bemporad, and M. Morari. *Predictive control for linear and hybrid systems*. Cambridge University Press, 2017.
- [75] J. B. Rawlings. Tutorial overview of model predictive control. *IEEE control systems magazine*, 20(3):38–52, 2000.
- [76] S. Levine and V. Koltun. Continuous inverse optimal control with locally optimal examples. *arXiv preprint arXiv:1206.4617*, 2012.
- [77] K. Mombaur, A. Truong, and J.-P. Laumond. From human to humanoid locomotion—an inverse optimal control approach. *Autonomous robots*, 28(3):369–383, 2010.
- [78] S. Boyd, L. El Ghaoui, E. Feron, and V. Balakrishnan. *Linear matrix inequalities in system and control theory*. SIAM, 1994.
- [79] M. Palan, S. Barratt, A. McCauley, D. Sadigh, V. Sindhvani, and S. Boyd. Fitting a linear control policy to demonstrations with a kalman constraint. In *Learning for Dynamics and Control*, pages 374–383. PMLR, 2020.
- [80] B. Amos, I. Jimenez, J. Sacks, B. Boots, and J. Z. Kolter. Differentiable mpc for end-to-end planning and control. In *Advances in Neural Information Processing Systems*, pages 8289–8300, 2018.
- [81] E. Pauwels, D. Henrion, and J.-B. Lasserre. Inverse optimal control with polynomial optimization. In *53rd IEEE Conference on Decision and Control*, pages 5581–5586. IEEE, 2014.
- [82] D. P. Bertsekas. Nonlinear programming. *Journal of the Operational Research Society*, 48(3): 334–334, 1997.
- [83] J. Lorraine, P. Vicol, and D. Duvenaud. Optimizing millions of hyperparameters by implicit differentiation. In *International Conference on Artificial Intelligence and Statistics*, pages 1540–1552, 2020.
- [84] A. Agrawal, B. Amos, S. Barratt, S. Boyd, S. Diamond, and J. Z. Kolter. Differentiable convex optimization layers. In *Advances in neural information processing systems*, pages 9562–9574, 2019.
- [85] A. Agrawal, S. Barratt, S. Boyd, and B. Stellato. Learning convex optimization control policies. *arXiv preprint arXiv:1912.09529*, 2019.
- [86] M. Blondel, Q. Berthet, M. Cuturi, R. Frostig, S. Hoyer, F. Llinares-López, F. Pedregosa, and J.-P. Vert. Efficient and modular implicit differentiation. *arXiv preprint arXiv:2105.15183*, 2021.
- [87] J. C. Dunn and D. P. Bertsekas. Efficient dynamic programming implementations of newton’s method for unconstrained optimal control problems. *Journal of Optimization Theory and Applications*, 63(1):23–38, 1989.
- [88] S. J. Wright. Solution of discrete-time optimal control problems on parallel computers. *Parallel Computing*, 16(2-3):221–237, 1990.
- [89] W. Li and E. Todorov. Iterative linear quadratic regulator design for nonlinear biological movement systems. In *ICINCO (1)*, pages 222–229. Citeseer, 2004.
- [90] D. Murray and S. Yakowitz. Differential dynamic programming and newton’s method for discrete optimal control problems. *Journal of Optimization Theory and Applications*, 43(3): 395–414, 1984.

- [91] A. Dosovitskiy, L. Beyer, A. Kolesnikov, D. Weissenborn, X. Zhai, T. Unterthiner, M. Dehghani, M. Minderer, G. Heigold, S. Gelly, et al. An image is worth 16x16 words: Transformers for image recognition at scale. *arXiv preprint arXiv:2010.11929*, 2020.
- [92] P. Ramachandran, N. Parmar, A. Vaswani, I. Bello, A. Levskaya, and J. Shlens. Stand-alone self-attention in vision models. *Advances in Neural Information Processing Systems*, 32, 2019.
- [93] A. Steiner, A. Kolesnikov, X. Zhai, R. Wightman, J. Uszkoreit, and L. Beyer. How to train your vit? data, augmentation, and regularization in vision transformers. *arXiv preprint arXiv:2106.10270*, 2021.
- [94] R. Frostig, V. Sindhwani, S. Singh, and S. Tu. trajax: differentiable optimal control on accelerators, 2021. URL <http://github.com/google/trajax>.
- [95] S. Pirk, E. Lee, X. Xiao, L. Takayama, A. Francis, and A. Toshev. A protocol for validating social navigation policies, 2022.
- [96] R. Likert. A technique for the measurement of attitudes. *Archives of psychology*, 1932.
- [97] H. Karnan, A. Nair, X. Xiao, G. Warnell, S. Pirk, A. Toshev, J. Hart, J. Biswas, and P. Stone. Socially compliant navigation dataset (scand): A large-scale dataset of demonstrations for social navigation. *IEEE Robotics and Automation Letters*, 2022.
- [98] M. Ahn, A. Brohan, N. Brown, Y. Chebotar, O. Cortes, B. David, C. Finn, K. Gopalakrishnan, K. Hausman, A. Herzog, et al. Do as i can, not as i say: Grounding language in robotic affordances. *arXiv preprint arXiv:2204.01691*, 2022.

## Appendix

### A Differentiable MPC

We provide some additional details regarding the learnable MPC, including the structure of the static cost and differentiation of the optimal solution w.r.t. the parameters of the cost neural networks.

**Static Cost Function:** Recall that the structure of our cost function inside the model predictive controller takes the form  $\bar{c}(\mathbf{x}, \mathbf{u}, t) + c_{\text{learn}}$  where  $c_{\text{learn}}(\mathbf{x}, \mathbf{u}; C_0, \theta)$  is the context-dependent residual cost. Let  $\mathbf{u} := (\mathbf{u}_v, \mathbf{u}_\omega)$  be the 2D control vector consisting of the body-aligned forward speed  $\mathbf{u}_v$  and turn rate  $\mathbf{u}_\omega$ , and let  $\mathbf{x} := (\mathbf{p}, \phi)$  be the state vector consisting of the 2D plane position  $\mathbf{p}$  and orientation  $\phi$ . The static cost function takes the form:

$$\bar{c}(\mathbf{x}, \mathbf{u}, t) := \sum_{i=1}^6 w_i \bar{c}_i(\mathbf{x}, \mathbf{u}, t) \quad (10a)$$

$$\bar{c}_1(\mathbf{x}, \mathbf{u}, t) := \mathbb{I}_{\mathbf{u}_v \geq 0} |\mathbf{u}_v|^4, \quad \bar{c}_2(\mathbf{x}, \mathbf{u}, t) := \mathbb{I}_{\mathbf{u}_v < 0} |\mathbf{u}_v|^4, \quad \bar{c}_3(\mathbf{x}, \mathbf{u}, t) := |\mathbf{u}_\omega|^4 \quad (10b)$$

$$\bar{c}_4(\mathbf{x}, \mathbf{u}, t) := \sum_{j=1}^{n_c} \text{ReLU}^2(\text{margin} - d_j(\mathbf{x})) \quad (10c)$$

$$\bar{c}_5(\mathbf{x}, \mathbf{u}, t) := \bar{w}_T(t) \|\mathbf{p} - \mathbf{g}\|^2, \quad \bar{c}_6(\mathbf{x}, \mathbf{u}, t) := \bar{w}_T(t) (1 - \cos(\phi - g_\phi)) \quad (10d)$$

$$\bar{w}_T(t) := \begin{cases} 1 & \text{if } t < T \\ \frac{T(1 + w_T)}{Tw_T + 1} & \text{if } t = T. \end{cases} \quad (10e)$$

where  $d_j(\mathbf{x})$  is the signed distance from the  $j^{\text{th}}$  collision-point on the robot body to the nearest obstacle, margin is a user-set margin threshold,  $\mathbf{g} \in \mathbb{R}^2$  is a 2D goal position,  $g_\phi$  is a goal orientation, and  $\{w_i\}_{i=1}^6, w_T$  are a set of non-negative weights. Thus, the static/hand-engineered cost function consists of an asymmetric control penalty, margin-offset collision penalty, and a time-weighted goal-reaching penalty.

**Tracking MPC:** The final policy action is determined as the solution to a secondary, non-learnable MPC problem (termed “tracking MPC”), taking the form of (1) but with the cost comprising of only the static portion, i.e.,  $\bar{c}$ . As defined above, this cost features a goal-reaching penalty. For the “higher-level” MPC problem (i.e., the problem solved by either Performer-MPC or RMPC), this goal is determined from problem context, e.g., a global waypoint. For the “tracking MPC” problem, this goal is set as an intermediate state extracted from the optimal state trajectory solution to the “higher-level” MPC problem. In the EP case, this goal is directly output by the EP policy. Using such a dual/tracking-MPC structure allows a more fair comparison between the three policies since the lowest-level control action is output in an identical manner.

**Jacobian of Optimal MPC solution:** The key tool for computing the desired Jacobian is the implicit function theorem, stated below (note: we suppress the dependence of the MPC cost function  $J_c$  on the context  $C_0$  for readability):

**Theorem A.1** (Implicit Function Theorem). *If in the neighborhood of  $(\mathbf{u}^*, \theta_k)$  where  $\nabla_{\mathbf{u}} J_c(\mathbf{u}^*, \theta_k) = 0$ , the Hessian  $\nabla_{\mathbf{u}}^2 J_c(\mathbf{u}^*, \theta_k)$  is non-singular, then we have:*

$$\partial_{\theta} \mathbf{u}^*(\theta_k) = - [\nabla_{\mathbf{u}}^2 J_c(\mathbf{u}^*, \theta_k)]^{-1} \nabla_{\theta, \mathbf{u}}^2 J_c(\mathbf{u}^*, \theta_k) \quad (11)$$

The Hessian term above need not be explicitly materialized, since by chaining Eqns 4 and 11, the VJP can be efficiently calculated as,

$$\nabla_{\theta} J_l(\mathbf{u}^*(\theta_k)) = - \left[ [\nabla_{\mathbf{u}}^2 J_c(\mathbf{u}^*, \theta_k)]^{-1} \nabla_{\mathbf{u}} J_l(\mathbf{u}^*(\theta_k)) \right]^T \nabla_{\theta, \mathbf{u}}^2 J_c(\mathbf{u}^*, \theta_k) \quad (12)$$

The term inside the large square brackets may be computed as the solution to the following quadratic problem:

$$\arg \min_{\delta \mathbf{v} := (\delta \mathbf{v}_0, \dots, \delta \mathbf{v}_{T-1})} \frac{1}{2} \delta \mathbf{v}^T \nabla_{\mathbf{u}}^2 J_c(\mathbf{u}^*, \theta_k) \delta \mathbf{v} + \delta \mathbf{v}^T \nabla_{\mathbf{u}} J_l(\mathbf{u}^*(\theta_k)),$$

which in turn decomposes into a TV-LQR problem [87] (Thm. A.1). Finally, the dot product with  $\nabla_{\theta, \mathbf{u}}^2 J_c(\mathbf{u}^*, \theta_k)$  may be computed by differentiating the co-state equations associated with the gradient  $\nabla_{\mathbf{u}} J_c(\mathbf{u}^*, \theta_k)$ .

## B Speed studies over various Performers’ architectures

We run speed studies over various Performer-MPC variants to choose the most suitable one for on-robot deployment characterized by strict latency constraints. The tests were run for  $100 \times 100$  resolution images and two architecture sizes: large and medium (details below).

**Large and medium architecture:** The large architecture consists of  $l = 6$  layers and  $h = 3$  heads with  $\text{mlpdim} = 1024$ . The medium architecture consists of  $l = 3$  layers and  $h = 1$  head with  $\text{mlpdim} = 64$ . Both apply GELU nonlinearity in the MLP-layers. For  $100 \times 100$  images, the large architecture has 24, 581, 732 parameters, and the medium architecture has 8, 334, 884 parameters.

**Tested Performer variants:** We test 13 different Performer versions: one Performer-ReLU and 12 Performer-Exps. For Performer-Exps, we test both redrawing and no-redrawing, as well as a range of different random projections (rps) including 8, 16, 32, 64, 128, and 256.

**Results:** Our first set of results with patch size  $5 \times 5$  is presented in Table 3 (we report there wall-clock time). To obtain the desired speed  $< 0.1\text{sec}$  per MPC call with the average number of MPC iterations around  $\text{nb} = 10$ , we look for time per MPC-iteration  $< 10\text{ms}$ . Because this requirement is satisfied by the medium-size Performer-ReLU variant, we deploy it as our vision backend on-robot. We then study the inference speed of this variant for different patch sizes and note that we can run it efficiently on robot with almost pixel-to-pixel ( $1 \times 1$  patch size) attention resolution (for completeness, we include Table 4 here again, where we report CPU-times to accurately distill time taken by the MPC from other factors such as I/O time).

## C Experimental Setup

We further provide details about our experimental setup.

### C.1 Robot Setup

Our robot can move at a linear speed between  $[-0.8, 0.8]\text{m/s}$ , and can rotate at an angular speed between  $[-1.2, 1.2]\text{rad/s}$ . The on-board software stack can perform SLAM (Simultaneous Localization And Mapping) and generate at each time step an occupancy grid with  $0.05 \times 0.05\text{m}$  cells (occupied or free) around the robot within  $[-7.5, 7.5]\text{m}$  of range for both  $x$  and  $y$  axis. For most experiments such as in tight spaces and blind corners, we clip the occupancy grid to  $[-2.5, 2.5]\text{m}$  ( $100 \times 100$  cells) since there is enough local information to make navigation decisions. Only for the pedestrian obstruction scenario we reduce the occupancy grid to  $[-4.5, 4.5]\text{m}$  ( $180 \times 180$  cells) so the human can be detected early to leave enough decision making time.

### C.2 Data Collection for Doorway Traversal

To learn to avoid local minima in the doorway traversal scenario, we use an artificial expert to generate 2000 training episodes. Each episode is generated by (1) randomly sampling a start configuration on one side of the door and a goal position on the other side, (2) running a coarse Dijkstra’s search to generate sparse global way points leading from the start through the doorway to the goal, and (3) feeding these way points on by one (i.e., using the solution of the last way point as the initial condition for the MPC solve for the next one) to an off-line MPC planner with 100 planning horizon and 200 maximum iterations (instead of 20 horizon and 20 iterations of the online MPC deployed on our robot). Such a heavy-duty planner requires too much computation to run onboard our robot.



Table 3: Full speed ablation tests for different variants of Performers with  $100 \times 100$  input images. The architecture deployed on the real robot is denoted in **bold** (Extension of Tab. 1).

model size	Performer type	redraw	nb rps	wall-clock time per MPC-iteration [ms]
<b>medium</b>	<b>ReLU</b>	<b>N/A</b>	<b>N/A</b>	<b>8.3</b>
medium	Exp	False	8	21.5
medium	Exp	False	16	21.6
medium	Exp	False	32	22.2
medium	Exp	False	64	23.6
medium	Exp	False	128	24.7
medium	Exp	False	256	26.8
medium	Exp	True	8	73.6
medium	Exp	True	16	67.6
medium	Exp	True	32	74.0
medium	Exp	True	64	75.0
medium	Exp	True	128	79.0
medium	Exp	True	256	81.6
large	ReLU	N/A	N/A	13.8
large	Exp	False	8	72.9
large	Exp	False	16	66.9
large	Exp	False	32	77.4
large	Exp	False	64	83.0
large	Exp	False	128	83.0
large	Exp	False	256	74.0
large	Exp	True	8	104.1
large	Exp	True	16	128.7
large	Exp	True	32	116.2
large	Exp	True	64	97.1
large	Exp	True	128	143.5
large	Exp	True	256	149.3

Table 4: Speed ablation over patch sizes for medium-sized Performer-ReLU with  $100 \times 100$  inputs.

patch sizes	$1 \times 1$	$2 \times 2$	$4 \times 4$	$5 \times 5$	$10 \times 10$
number of params (M)	15.7	9.93	8.50	8.33	8.16
CPU-time per MPC-iteration (ms)	11.3	2.6	2.3	1.5	0.5

For the 2000 expert trajectories of 100 horizon, we apply a moving window of size 20 and extract 80 trajectories of 20 horizon, but keep the original goal of the 100-horizon trajectory on the other side of the wall, as expert demonstration data for the Performer-MPC to learn (the starting locations of these expert trajectories are shown in Fig. 7, with a few rare failure cases of the offline planner displayed by a few erratic points).

### C.3 Data Collection for Highly Constrained Maneuvers

To learn agile maneuvers in the highly constrained obstacle course, we collect data from a human expert via joystick teleoperation. The human expert teleoperates the robot to randomly navigate in a collision-free manner in the cluttered obstacle course (Fig. 3 b). The entire demonstration lasts around 30 minutes. For each data point, we set the goal as the 200-th future state on the demonstrated trajectory. At around 60Hz state rate and 0.5m/s driving speed, the goal is roughly 2m in front of the robot. In addition to this demonstration of desirable navigation behavior, we further collect about 10 minutes of demonstration starting from failure locations, e.g., where the robot is stuck and unable to recover from such situations, to address the distribution shift problem.

### C.4 Data Collection for the Two Social Scenarios

We defer the data collection details for the two social scenarios to Appendix D after the social scenarios are formally defined to facilitate understanding.

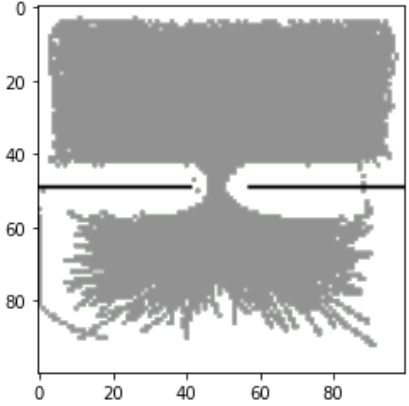


Figure 7: Expert Demonstrations Generated by an Off-Line MPC Planner Guided by a Dijkstra’s Global Planner ( $x$  and  $y$  axis units are in occupancy grid cells).

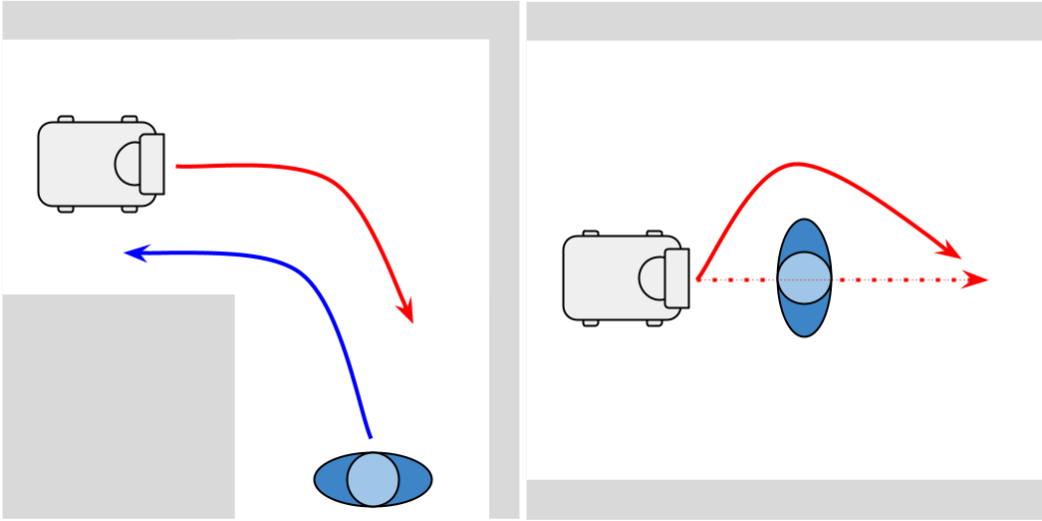


Figure 8: Social Navigation Scenarios. (a) In the blind corner scenario, robots should swing wide or slow down to avoid possible collisions with approaching humans who are not visible. (b) In the pedestrian obstruction scenario, the robot should go around the visible obstructing human with a comfortable passing distance.

### C.5 Training Time

Our bilevel optimization takes around 0.36 seconds per iteration, i.e., a forward inference pass and a backward training pass (Fig. 2) to update the learnable parameters  $\theta$  (Eqn. 2) on four TPUs. As shown in Fig. 4, it takes around 15, 60, 1.5, and 10 hours for our Performer-MPC model to converge for the doorway traversal, highly constrained maneuvers, blind corner, and pedestrian obstruction scenarios, respectively.

## D Social Navigation Evaluation

To make evaluation of social navigation policies well-defined, realistic, scalable and repeatable, we use a social navigation benchmark based on a set of human-robot interaction scenarios to be evaluated using user surveys previously designed by Pirk et al. [95]. This benchmark consists of scenarios with well-defined roles and expected behavior for both humans and robots, along with a series of questions for human raters with answers defined on a five-level Likert scale [96]. To provide a concise metric for comparing policies, we average the answers to these questions into a

Blind Corner		Pedestrian Obstruction		General Questions	
BC1	The robot moved to avoid me.	PO1	The robot moved to avoid me.	G1	The robot adhered to social norms.
BC2	The robot stopped to let me pass.	PO2	The robot maintained a safe and comfortable distance.	G2	I would feel comfortable around the robot in this encounter.
BC3*	The robot nearly collided with me.	PO3*	The robot nearly collided with me.	G3	All things considered, I rate the robot motion as:
BC4*	I had to move around the robot	PO4	It was clear what the robot wanted to do.		Very Poor / Poor / Neutral / Good / Very Good.

Table 5: Questions for Each Social Scenario. A star indicates a question is negative, so that a ‘Strongly Disagree’ result should be aligned with ‘Strongly Agree’ for a positive question.

social navigation score reported in the main body of the paper (Fig. 6). This section justifies that choice by describing this social navigation protocol and the results of our experiments in more detail.

### D.1 Social Navigation Scenarios

Crucially for our purposes, this protocol can be used to generate trajectories and evaluate whether they meet the scenario’s social criteria, enabling us to create curated datasets of expert trajectories which score highly on our benchmark. For training Performer-MPCs, we chose two scenarios:

- **blind corner** (Fig. 8a), in which a robot is expected to apply some strategy (such as slowing down or swinging wide) to reduce the likelihood of collision with a possible unseen pedestrian coming around a corner.
- **pedestrian obstruction** (Fig. 8b), in which the robot is expected to drive around a human obstructing its path, while respecting the human’s comfort distance.

Table 5 details the questions used to evaluate each scenario, along with a set of scenario-independent general questions. For most questions, the Likert scale is implemented as Strongly Disagree, Disagree, Neutral, Agree, Strongly Agree, except for question G3, which evaluates overall performance with Very Poor, Poor, Neutral, Good, Very Good.

### D.2 Collecting Expert Demonstrations

We use the scenario definitions to collect a variety of expert demonstration datasets. For both scenarios, we collect around 30 episodes each scenario, which prove sufficient for training Performer-MPC. Note compare to taking visual RGB camera input which requires over 700 episodes each scenario [95], Performer-MPC takes occupancy grids as input and requires substantially smaller amount of data.

For our social scenario data collection, human expert trajectories are collected by individuals trained as both participants and evaluators of the social scenarios, who attempt in their runs to guide the robot according to the social norms defined in the scenarios. In turn, our evaluation of Performer-MPC against baselines in these scenarios uses the same definitions and questionnaires which guide the trajectories; thus our experimental results gauge how well Performer-MPCs can successfully navigate with respect to social norms whose cost functions are difficult to explicitly design.

For **pedestrian obstruction**, we discover that both Performer-MPC and EP tend to memorize the building configurations of the training environment (e.g., walls, chairs, and tables) and sometimes do not respond to the human properly during deployment. Therefore, we augment the existing training data by randomly shuffling the background (i.e., randomly removing or adding obstacle pixels to the surrounding area, but keeping the space around the robot-human interaction point intact). We posit that such data augmentation may not be necessary when we scale up our data collection to different building configurations, and more importantly, adding extra information to distinguish humans from obstacles (e.g., human detection, tracking, and prediction). For the **blind corner** scenario, swinging wide to avoid the inner side of the corner is part of the desired learning process, therefore such augmentation is not necessary.

We also randomly select goal locations between behind the human and the final robot position of each episode for the **pedestrian obstruction** scenario to improve the model’s robustness against

different goals. Again, for `blind corner`, we find such augmentation not necessary and simply select the 300-th future state on the demonstrated trajectory as goal for each data point. In this way, most data points have a goal behind the corner. We posit that these two data augmentation techniques contribute to the much longer training time for `pedestrian obstruction` than that for `blind corner` (Fig. 4).

### D.3 Human Evaluation Pilot Study

To evaluate the performance of our social navigation policies, we conduct a pilot study, gathering both participant and observer perspectives using the scenario questionnaires. Due to covid-19 restrictions and limited availability of participants for in-person user study participation (N=9), we ran this pilot study with members of our research team. In this pilot study, we aim to address the research question: *How well does our Performer-MPC social navigation policy perform on our social navigation metrics when compared against RMPC and EP?*

Beyond that research question, we also aim to explore several other variables. First, we want to see how these policies would perform when comparing previously seen environments (i.e., environments where the training set is collected) vs. unseen environments (i.e., novel environments not in the training set). Second, we want to examine how direct interactants (1st person) vs. bystanders (3rd person) would rate the robot’s social navigation performance because we hypothesize that 1st person responses might be stronger, especially when it comes to perceptions of comfort and safety. Third, we want to test the policies’ performances across at least two different social navigation scenarios, starting with `blind corner` and `pedestrian obstruction`.

As this is a large set of variables (navigation policy, performing in seen vs. unseen environments, measuring from 1st vs. 3rd person perspectives, and navigating in two different social navigation scenarios) and we have a very limited set of research study participants, we opt to run this as an exploratory pilot study, not as a fully controlled, counterbalanced, human subjects experiment. Altogether we run 120 sessions, gathering 240 sets of questionnaire responses from 1st and 3rd person perspectives in the course of one day in June 2022 on our campus (N=9). To minimize possible bias, neither pedestrians nor observers are aware of what policy is being tested during each episode, and the ordering of policies is randomized.

### D.4 Evaluating Social Navigation Performance Factors

To assess the relationship between people’s responses to our social navigation questionnaire items, we run principal component analyses (using varimax rotations) to see if the variables really do hang together. We also run reliability analyses to see if those items that load onto a single factor are indeed reliable measures of an underlying factor.

- `blind corner`: The three general questions in this set (Questions G1-G3) create a highly reliable factor, Cronbach’s alpha = .92 (N=120). When we run PCA on the questions that are specific to the `blind corner` scenario (Questions BC1-B4), one of the items does not correlate strongly with the other three (BC2: The robot stopped to let me pass).
- `pedestrian obstruction`: We find that the three general social navigation performance questions (Questions G1-G3) create a highly reliable factor, Cronbach’s alpha = .99 (N=240). For the four questions specific to the `pedestrian obstruction`, we find that all four questions (Questions PO1-PO4) also create a highly reliable factor, Cronbach’s alpha = .97 (N=120).

Because these results show most these variables are highly correlated, we average them into a “social navigation score” for presenting our results in the main body of the paper concisely. The following section presents the detailed results of the social questionnaire evaluation.

### D.5 Pilot Study Results

As we are unable to fully balance the experiment design (e.g., getting each of our participants to try out each of the 24 experiment conditions once), we cannot satisfy the statistical analysis assumptions of repeated measures ANOVAs. As such we are reporting upon the descriptive statistics (means and standard errors) of our pilot study data, but we recommend interpreting these results as pilot study findings, not statistically significant findings that indicate causal relationships.

Policy Tested	Eval Cond	BC1 Avoided Human	BC2 Stop for Human	BC3 No Fear Collision	BC4 No Dodge	G1 Social Norms	G2 User Comfort	G3 Perceived Quality	Social Score	Failed Episode	Num Samples
Regular MPC	Seen <i>Std. Err.</i>	1.65 0.08	2.00 0.11	1.75 0.14	1.95 0.15	1.90 0.12	2.00 0.13	1.90 0.12	1.88	0%	60
	Unseen <i>Std. Err.</i>	2.10 0.09	2.15 0.09	2.50 0.11	2.05 0.14	2.60 0.11	2.60 0.11	2.65 0.10	2.38	0%	60
Explicit Policy	Seen <i>Std. Err.</i>	3.90 0.14	1.90 0.14	4.65 0.06	4.70 0.06	4.65 0.06	4.70 0.06	4.60 0.06	4.16	0%	60
	Unseen <i>Std. Err.</i>	3.40 0.18	1.80 0.14	4.00 0.17	3.70 0.20	2.95 0.17	3.25 0.18	3.10 0.18	3.17	20%	60
Performer-MPC	Seen <i>Std. Err.</i>	3.20 0.17	1.75 0.07	4.60 0.10	4.35 0.10	4.30 0.08	4.45 0.09	4.50 0.09	3.88	0%	60
	Unseen <i>Std. Err.</i>	3.75 0.13	1.90 0.08	4.60 0.06	4.20 0.09	4.15 0.10	4.25 0.09	4.25 0.08	3.87	0%	60

Table 6: Social Navigation Questionnaire Results for blind corner.

Policy Tested	Eval Cond	PO1 Avoided Human	PO2 Comfort Distance	PO3 No Fear Collision	PO4 Motion Legible	G1 Social Norms	G2 User Comfort	G3 Perceived Quality	Social Score	Failed Episode	Num Samples
Regular MPC	Seen <i>Std. Err.</i>	1.74 0.13	1.42 0.07	1.47 0.08	1.63 0.11	1.47 0.07	1.53 0.07	1.58 0.07	1.55	0%	60
	Unseen <i>Std. Err.</i>	1.95 0.21	1.85 0.20	2.00 0.19	2.00 0.17	2.00 0.19	2.00 0.19	1.95 0.19	1.96	0%	60
Explicit Policy	Seen <i>Std. Err.</i>	4.45 0.08	4.15 0.12	4.40 0.10	3.80 0.12	4.15 0.10	4.30 0.10	4.15 0.10	4.20	5%	60
	Unseen <i>Std. Err.</i>	4.30 0.16	4.15 0.15	4.05 0.15	3.80 0.17	4.10 0.15	4.10 0.15	4.05 0.15	4.08	5%	60
Performer-MPC	Seen <i>Std. Err.</i>	4.57 0.07	4.38 0.10	4.48 0.10	4.19 0.07	4.29 0.12	4.38 0.08	4.43 0.08	4.39	0%	60
	Unseen <i>Std. Err.</i>	4.00 0.19	4.15 0.16	4.15 0.16	4.05 0.15	4.15 0.16	4.15 0.16	4.05 0.15	4.10	0%	60

Table 7: Social Navigation Questionnaire Results for pedestrian obstruction.

- blind corner (Tab. 6): The best performing policy on blind corner is the EP policy in the seen condition, with a combined score of 4.16 and individual questionnaire scores equal to or higher than both other policies. However, EP does not generalize well to the unseen condition, suffering a 20% failure rate and a drop in social score to 3.17; differences between the performance of these policies on individual questions are generally greater than the standard errors of these policies, potentially indicating a real difference that could be teased out with a larger study. In contrast, Performer-MPC generalizes well, with scores on seen and unseen of 3.88 and 3.87 respectively, with individual questions generally showing greater differences. RMPC is the worst performing policy in the overall social score and on most individual questions, except BC2, “The robot stopped to let me pass,” on which it is slightly superior due to stopping for users. However, this illuminated issues on question BC2, which we discuss further below.
- pedestrian obstruction (Tab. 7): The best performing policy on pedestrian obstruction is Performer-MPC in the seen condition with overall social score of 4.39, with a relatively small drop to 4.10 in the unseen condition. EP also performs well with scores in seen and unseen of 4.20 and 4.08, respectively, though it fails to complete the task 5% of the time in both conditions. While the difference in seen performance of these policies is typically greater than the standard error of their performance, potentially indicating a real difference which could be teased out with a larger study, this is not true in the unseen case. RMPC is the worst performing policy in both social score and individual questions. Results within questions, between questions and within policies under given conditions are generally more consistent for pedestrian obstruction than blind corner.

Overall, we interpret these results to indicate that Performer-MPC has better generalization than EP and is comparable in social navigation performance to EP, and that both of those policies are superior to RMPC at social navigation. The social navigation score results presented in the main body of the paper are consistent with this detailed analysis.

However, the outlier question BC2 is worth further discussion. All other questions in our survey hang together to create highly reliable factors, but BC2 does not, and show lower scores for both Performer-MPC and EP, which otherwise score highly on the social navigation questionnaire. Discussion with the participants and analysis of robot behaviors in the episodes reveal that this question inadvertently prescribes a solution: that the robot should stop at the blind corner. However, our expert training demonstrations incorporate a different solution: swinging wide at the corner to avoid collisions, which our human robot drivers determine is the preferred solution based on the navigation speed and stopping distance of the robot. In contrast, RMPC, while not scoring well on most social questions, nevertheless stop for the user, giving it an artificially high score on this question even though its behavior is not very social due to stopping very close to the user. While we report the results of this question for completeness, for future work we plan to craft questions which evaluate social navigation without prescribing a solution.

## D.6 Limitations and Future Work

This paper focuses on whether Performer-MPC can successfully learn from expert demonstrations derived from real-world scenarios and then be successfully deployed in those scenarios on-robot. Therefore, we select a limited set of social scenarios which enables us to evaluate this research question. These scenarios are necessarily limited to those which can be detected from the occupancy grid, which preclude the use of the visual gesture-based scenarios proposed by Pirk et al. [95]. Furthermore, data for these scenarios are collected by a limited number of human experts, and the policies for each scenario are trained separately. In future work, we plan to expand to a wider range of scenarios collected by a broader range of experts, and to train policies to solve sets of scenarios rather than a single scenario.

The user evaluation pilot study is a first step toward developing a more robust user study protocol for evaluating future versions of social navigation policies. Our pilot study is limited by its use of research team members as study participants; their perspectives on social navigation behavior are quite influenced by their experience with operating and running tests on these robots in their work. In the future, we will recruit user study participants from people, who are not part of our research team. Second, our pilot study is not properly balanced so we cannot run the usual statistical analyses necessary to evaluate the statistical significance of the effects we observed. Instead, we report upon the descriptive statistics for this paper and we will run a full user study as a next step in this research project. In future user studies, we will focus upon more targeted research questions so that the experiments are simpler to run, analyze, and interpret, and will ensure these questions focus on quality of social navigation without tying evaluation quality to mimicking a specific solution behavior.